(2)



OFFICE OF NAVAL RESEARCH

Contract N00014-83-K-0470-P00003

R&T Code NR 33359-718

Technical Report No. 90

# An Electrochemical and Spectroelectrochemical Analysis of the Oxide / p-INP Semiconductor Surface Using FTIR and Raman Scattering Spectroscopies

by

J. Li and S. Pons

Prepared for publication in J. Electroanal. Chem.

Department of Chemistry
University of Utah
Salt Lake City, UT 84112



July 15, 1988

SECURITY CLASSIFICATION OF THIS PAGE

# REPORT DOCUMENTATION PAGE

| | |
|---|---|
| 1a. REPORT SECURITY CLASSIFICATION: Unclassified | 1b. RESTRICTIVE MARKINGS |
| 2a. SECURITY CLASSIFICATION AUTHORITY | 3. DISTRIBUTION / AVAILABILITY OF REPORT: Approved for public release and sale. Distribution unlimited. |
| 2b. DECLASSIFICATION / DOWNGRADING SCHEDULE | |
| 4. PERFORMING ORGANIZATION REPORT NUMBER(S): ONR Technical Report No. 90 | 5. MONITORING ORGANIZATION REPORT NUMBER(S) |
| 6a. NAME OF PERFORMING ORGANIZATION: University of Utah; 6b. OFFICE SYMBOL (If applicable) | 7a. NAME OF MONITORING ORGANIZATION |
| 6c. ADDRESS (City, State, and ZIP Code): Department of Chemistry, Henry Eyring Building, Salt Lake City, UT 84112 | 7b. ADDRESS (City, State, and ZIP Code) |
| 8a. NAME OF FUNDING / SPONSORING ORGANIZATION: Office of Naval Research; 8b. OFFICE SYMBOL (If applicable) | 9. PROCUREMENT INSTRUMENT IDENTIFICATION NUMBER: N00014-83-K-0470-P00003 |
| 8c. ADDRESS (City, State, and ZIP Code): Chemistry Program, Code 1113, 800 N. Quincy Street, Arlington, VA 22217 | 10. SOURCE OF FUNDING NUMBERS: PROGRAM ELEMENT NO. / PROJECT NO. / TASK NO. / WORK UNIT ACCESSION NO |

11. TITLE (Include Security Classification): **An Electrochemical and Spectroelectrochemical Analysis of the Oxide / p-INP Semiconductor Surface Using FTIR and Raman Scattering Spectroscopies**

12. PERSONAL AUTHOR(S): J. Li and S. Pons

| | | | |
|---|---|---|---|
| 13a. TYPE OF REPORT: Technical | 13b. TIME COVERED: FROM 9/87 TO 7/88 | 14. DATE OF REPORT (Year, Month, Day): July 05, 1988 | 15. PAGE COUNT: 24 |

16. SUPPLEMENTARY NOTATION

| 17. COSATI CODES | | | 18. SUBJECT TERMS (Continue on reverse if necessary and identify by block number) |
|---|---|---|---|
| FIELD | GROUP | SUB-GROUP | Spectroelectrochemistry, indium phosphide |
| | | | |
| | | | |

19. ABSTRACT (Continue on reverse if necessary and identify by block number)

Attached.

| | |
|---|---|
| 20. DISTRIBUTION / AVAILABILITY OF ABSTRACT: ☒ UNCLASSIFIED/UNLIMITED ☐ SAME AS RPT ☐ DTIC USERS | 21. ABSTRACT SECURITY CLASSIFICATION: Unclassified |
| 22a. NAME OF RESPONSIBLE INDIVIDUAL: Stanley Pons | 22b. TELEPHONE (Include Area Code): (801)581-4760; 22c. OFFICE SYMBOL |

DD FORM 1473, 84 MAR — 83 APR edition may be used until exhausted. All other editions are obsolete. SECURITY CLASSIFICATION

## ABSTRACT

Raman scattering and FTIR reflectance spectroscopies have been used to examine p-InP/oxide surfaces. The thin anodic oxide film grown in pH 6 tartaric acid solutions is found to be primarily indium dihydrogen phosphate. This layer gives rise to an appreciable reduction in band bending (as much as 300 mV) which is similar to that obtained by open circuit photovoltage measurements. The photocurrent–voltage behavior of p-InP/oxide shows that the growth of anodic oxide at p-InP introduces significant surface states which act as surface recombination centers.

*J. Electroanal. Chem.*, 00 (1987) JEC09144
Elsevier Sequoia S.A., Lausanne – Printed in The Netherlands

# AN ELECTROCHEMICAL AND SPECTROELECTROCHEMICAL ANALYSIS OF THE OXIDE/p-INDIUM PHOSPHIDE SEMICONDUCTOR SURFACE USING FOURIER TRANSFORM INFRARED AND RAMAN SCATTERING SPECTROSCOPIES

JIANGO LI and STANLEY PONS *

*Department of Chemistry, University of Utah, Salt Lake City, UT 84112 (U.S.A.)*

(Received 25th November 1986; in revised form 23rd February 1987)

## ABSTRACT

Raman scattering and FTIR reflectance spectroscopies have been used to examine p-InP/oxide surfaces. The thin anodic oxide film grown in pH 6 tartaric acid solutions is found to be primarily indium dihydrogen phosphate. This layer gives rise to an appreciable reduction in band bending (as much as 300 mV) which is similar to that obtained by open circuit photovoltage measurements. The photocurrent–voltage behavior of p-InP/oxide shows that the growth of anodic oxide at p-InP introduces significant surface states which act as surface recombination centers.

## INTRODUCTION

Considerable interest has been shown in recent years in the compound semiconductor p-InP because of its importance in application in semiconductor electronic devices and photoelectrochemical solar cells. The efficiency and performance of these devices depend very critically on the surface preparation. For example, fabrication of inversion-layer metal-insulated-semiconductor field-effect transistors (MISFETs) on p-InP requires surfaces grown oxides with good insulating properties. With respect to the InP photoelectrochemical solar cell (PEC) device, surface quality again determines success in high efficiency. Heller et al. [1] have investigated the pathways by which p-InP photocathodes for hydrogen evolution is effected; in particular they have investigated how platinum incorporation modifies the ability of p-InP to generate hydrogen efficiently with a small external bias voltage. Surprisingly it seems not only possible but also necessary to have a thin oxide film present during hydrogen evolution in order to maintain long term photocathode stability.

* To whom correspondence should be addressed.

0022-0728/87/$03.50 

The remarkable stability of this oxide film allows the cell to be operated in strongly acidic solutions (e.g. in 3 *M* HCl). Heller et al. [2] have therefore attempted to find optimum conditions for the formation of the oxide. One successful system has been the treating of the electrode with alkaline peroxide and KCN. Prior to these experiments, less systematic work has been performed on p-InP demonstrating enhancement of PEC performance. Such studies have, however, been performed on solid-state MOS devices, which is well known in many respects to be analogous to liquid junction PEC cells. Several methods for formation of an oxide film on p-InP. including anodic oxidation [3], thermal oxidation of p-InP [4] and chemical vapor deposition (CVD) of $SiO_2$ [5] or $Al_2O_3$ [6] have been studied. Due to the low decomposition temperature for p-InP [7], the temperature for the thermal processes is limited to comparatively low values. From this point of view, anodic oxidation has an advantage in that it can be performed at room temperature. It has therefore become a popular surface oxide film preparation method for electrochemical and other studies of either solid-state devices or liquid junction solar cells.

The design of experiments to enhance efficiency of a p-InP photocathode by preparation of an anodic oxide film in various electrolytes is, however, largely empirical and detailed surface characterization of the semiconductor surface is important and necessary in order to determine the role of oxide film. Lewerenz et al. [8] have used spectroscopic ellipsometry and low-energy (He) ion-scattering spectroscopy to show that a hydrated film of $In_2O_3$ is formed on p-InP by acid or bromine methanol etching procedures. Wilmsen and co-workers [9,10] have presented Auger and ESCA analysis of the anodic oxide composition on p-InP, demonstrating the oxide of p-InP is composed of $In_2O_3$ and $P_2O_5$. Yamamoto et al. [11] have examined the composition and structure of oxide on p-InP with reflection electron diffraction illustrating relations between anodic oxide preparation conditions and the electrical properties. In addition to studies on other semiconductors, Sakashita et al. [12] have recently applied laser Raman backscattering techniques to study the composition of the anodic oxide film on HgTe. Raman scattering (RS) is not only a probe to identify the oxide film on semiconductor, but also has proven to be a useful technique for obtaining gain information about surface electronic fields and the space-charge region (SCR) from the surfaces of zincblend-type semiconductors [13,14]. In this paper, we report results of the application of Fourier transform infrared spectroscopy to identify the composition and structure of the thin anodic oxide film on p-InP and systematic studies of electrical and photoelectrochemical properties of the p-InP/xodie surface by Raman scattering spectroscopy.

## EXPERIMENTAL

A Zn-doped p-InP single crystal wafer purchased from Crystal Comm Inc. had a doping density of $6 \times 10^{16}$ $cm^{-3}$, a surface orientation of (100) and a resistivity of 1.2 Ω cm. The electrodes for Raman scattering and electrochemical measurements were made of 5 × 5 mm square crystals and the one for FTIR measurements was a 10 mm diameter disk. The ohmic contact to the crystal was made with In + Zn (95 + 5%) alloy and mounted on a glass electrode holder with epoxy cement. Prior

to anodization, the electrode surface was polished with 0.3 $\mu$m alumina polishing powder on a cloth sheet to a mirror finish and afterward etched in 2% bromine/methanol or in a 6 : 1 : 1 : 1 $HNO_3 + HCl + HClO_4 + CH_4COOH$ mixed acid solution. The anodic oxidation of the p-InP surface was accomplished by cycling the p-InP electrode from $-0.3$ V to varying positive potential limits (0.4 to 0.7 V vs. SCE) for 5 scans at a sweep rate of 20 mV $s^{-1}$ in a 3% tartaric acid + propylene glycol (1 : 3 ratio, buffered by $NH_4OI$. › pH 6). The electrochemical measurements were performed in a conventional three-electrode component cell which had a quartz window at the bottom parallel to the semiconductor electrode surface. A saturated calomel reference electrode was used in aqueous electrolyte experiments. The reference electrode used in non-aqueous electrolyte was a silver wire in contact with a solution of $10^{-2}$ *M* $AgNO_3$ and 0.1 *M* tetra-n-butylammonium fluoroborate (TBAF) in acetonitrile. Platinum was used for the counter electrode. Acetonitrile (Caledon HPLC grade) was dried over Woelm neutral alumina before use.

Electrochemical experiments were performed with a JAS Instrument Systems, Inc. potentiostat and waveform generator. The cell was placed in a matte-black painted and ground-shielded aluminum cage to minimize capacitatively coupled noise and the interference of ambient light in the laboratory. The differential capacitance measurements were performed with the equipment mentioned above and an Ithaco Model 3961 two phase lock-in amplifier. A sine wave with 6 mV pp was superimposed on a slow ramp ($\nu$ = 20 mV $s^{-1}$) which was applied to the p-InP electrode.

Raman scattering spectra were measured using the 514.5 nm line of an $Ar^+$ laser, and a Spex double monochromator Raman spectrometer. The configuration of the measurements was a conventional 90° scattering geometry and the direction of the propagation of the incident beam was at an angle of 75° with respect to the normal to the electrode surface. The laser beam (~ 50 mW) was slightly defocussed on the electrode surface to prevent local overheating.

The infrared reflectance spectra were obtained with an IBM FT-98 vacuum spectrometer modified for surface studies and described elsewhere [15]. A KBr beamsplitter and a KBr optical bench window were employed in the measurements. The infrared detectors used in these experiments were cooled HgCdTe and deuterated triglycine sulfate detectors. The interferograms were recorded at a resolution of 8 $cm^{-1}$ while the optical bench was under vacuum. The infrared reflectance spectra shown in the figures were obtained by ratioing the average of 2048 scans taken at each of two electrode surfaces. Taking one spectrum of a prepared electrode surface as reference, bands in the spectra extending down represent vibrational modes of species predominating at the other prepared surface, while the bands pointing up correspond to those predominant at the reference surface.

All Raman scattering and FTIR reflectance spectra of the prepared pInP electrode surfaces were made ex situ. After preparation, they were rinsed in triply distilled water and clean acetone, and dried in a nitrogen gas stream. The sample chambers in the Raman and FTIR spectrometers were purged with dry nitrogen.

## RESULTS AND DISCUSSION

The photocurrent–voltage behavior of the semiconductor electrode is affected by the location of the band edges. With respect to p-InP photocathodes, the shifts in the position of the band edge are related to the surface preparation methods. Figures 1–3 illustrate in the Mott–Schottky plots that the flat-band potential depends on the etching solution and etching time. For the p-InP surface etched in 6 : 1 : 1 : 1 $HNO_3$ + HCl + $HClO_4$ + $CH_3COOH$ acid, the differential capacitance–potential curves of the forward potential scan overlapped that of the reverse scan at a sweep rate of 20 mV $s^{-1}$ in the dark and the flat-band potential was independent of the electrode prepolarization. A shift of flat-band potential, ~ 90 mV, shown from the intercepts of the Mott–Schottky plots in Fig. 1 occurred after prolonged etching. This positive shift in the flat-band potential decreased and finally reached a constant value of +0.29 V vs. $Ag/Ag^+$ whenever the etching time was longer than 1 min.

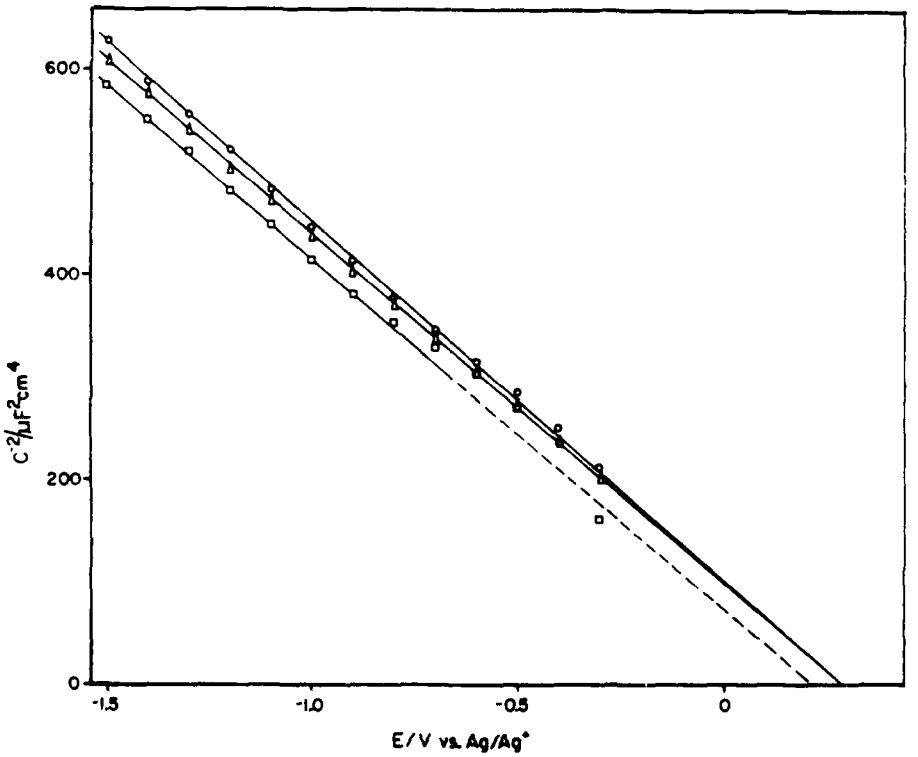


Fig. 1. Mott–Schottky plots for p-InP in 0.1 *M* TBAF + acetonitrile, $f = 1000$ Hz, electrode etched in 6:1:1:1 nitric + perchloric + acetic + hydrochloric acid for (□) 10 s; (△) 20 s; (○) 30 s.

The band edge shift of an p-InP surface etched in 2% $Br_2 + CH_3OH$ was not as evident as that observed at mixed acid etched surface. In addition the hysteresis between the forward and reverse scans on the differential capacitance—potential curves were observed in the first cycle but not in successive cycles. Since the capacitance measurements were carried in dry acetonitrile electrolyte, we may suggest that the hysteresis was due to a chemical transformation of the surface brought about durnng the first forward scan rather than a change in surface composition. The value of the flat-band potential of p-InP etched in $Br_2 + CH_3OH$ is 0.25 V vs. $Ag/Ag^+$, less positive than that of p-InP etched in the mixed acid (Fig. 3).

After pre-etching in the mixed acids or the $Br_2 + CH_3OH$, p-InP was oxidized in tartaric acid + propylene glycol by controlled positive limit potential cycling. The anodic oxidation current was observed to fall in successive potential scans indicating that a passivating and resistive oxide film grew with potential cycling. The integrated charge consumed for the oxide film, as calculated from the cyclic voltammogram, indicates that only a few monolayers of oxide are formed. However, Mott–Schottky plots with different positive limits of anodic oxidation demonstrate a significant change in the position of band edges (Figs. 2 and 3). The plateau in the

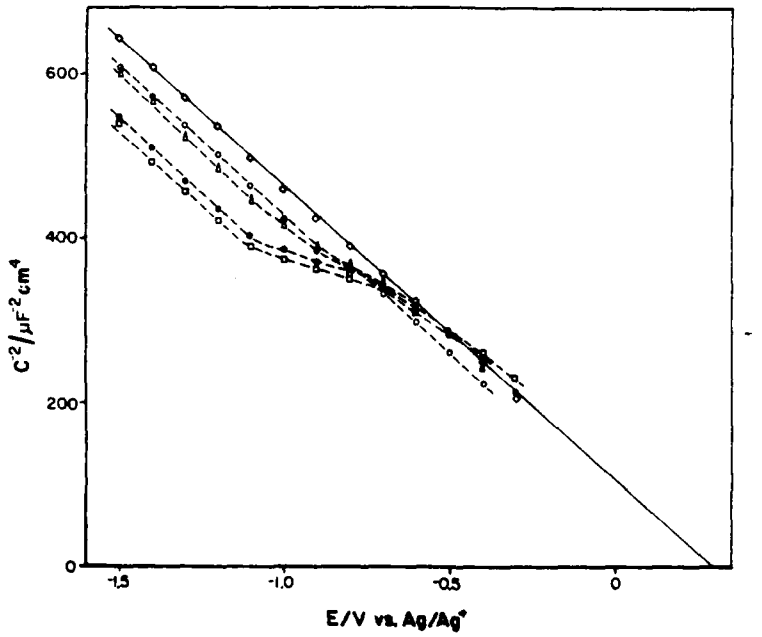


Fig. 2. Same as Fig. 1 except etched in acid bath (◇) and then anodically oxidized in 3% tartaric acid from −0.4 V vs. SCE to (○) +0.4 V; (△) +0.5 V; (●) +0.6 V; and (□) +0.7 V.

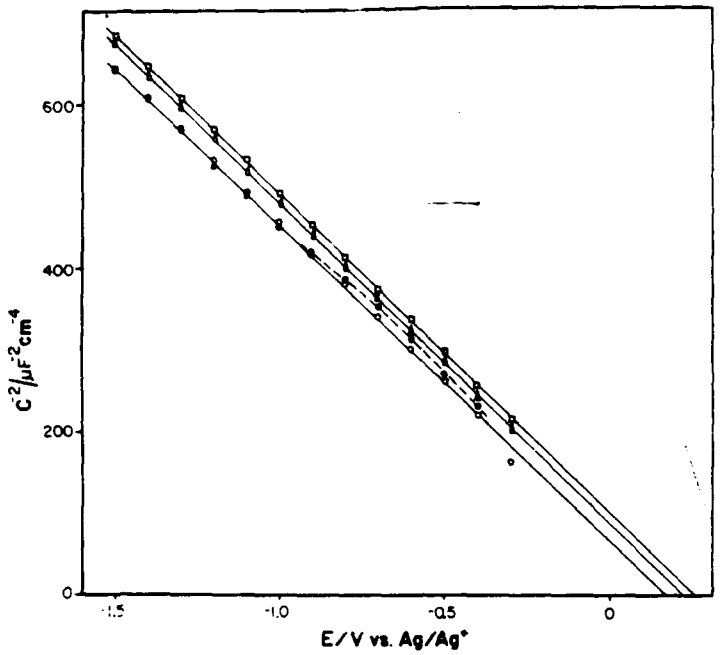


Fig. 3. Same as Fig. 1 except (□) etched in $Br_2$ + MeOH for 15 s; (△) oxidized in 3% tartaric acid from −0.4 to +0.4 V vs. SCE; (○) oxidized in 3% tartaric acid from −0.4 to +0.5 V vs. SCE; (●) oxidized in 3% tartaric acid from −0.4 to +0.7 V vs. SCE.

Mott–Schottky plot is characteristic evidence of Fermi level pinning. Extrapolating the plot in the large bandbending potential range gives a negative flat-band shift as large as 330 mV in the case of the electrode oxidized at a positive limit oxidation potential of 0.7 V vs. SCE. The same trend with smaller shifts in flat-band potential was observed at the anodically oxidized p-InP pre-etched in $Br_2 + CH_3OH$.

Figure 4 shows the Raman scattering spectrum measured at the mechanically polished p-InP surface. Two bands were observed at 284 $cm^{-1}$ and 349 $cm^{-1}$, respectively. The dominant first-order scattering process in semiconductors is due to optical phonons, which are either the longitudinal optical (LO) phonons or the transverse optical (TO) phonons. One can change the energy of the phonon that satisfy the conservation requirements and thus shift the band location in the spectrum of the scattered light by changing the elastic properties of the crystal through stress or other lattice disordering. Raman scattering spectra give more insight into the surface properties of the semiconductor electrodes. The TO and LO optical phonon modes have been reported as TO : 304 $cm^{-1}$ and LO : 346 $cm^{-1}$ for n-InP (100) [14]. We assign the 284 $cm^{-1}$ and 349 $cm^{-1}$ band as TO and LO phonon modes for our p-InP samples. The discrepancy between the reported and

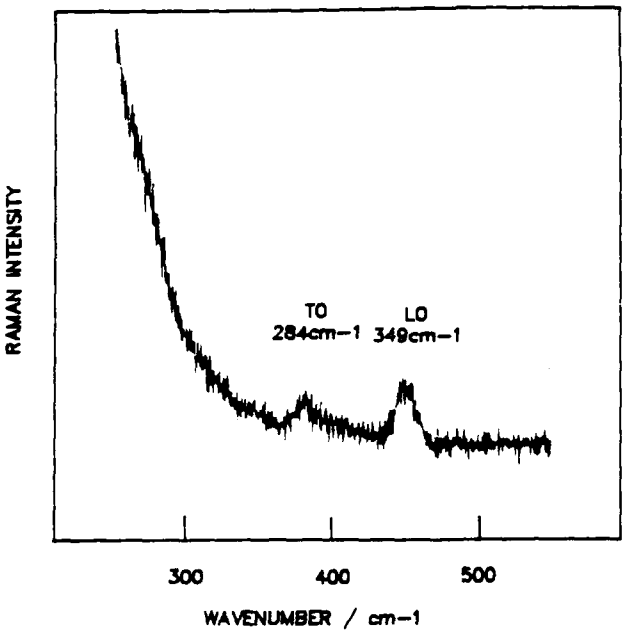


Fig. 4. Raman spectrum of p-InP polished with 0.3 μm alumina to a mirror finish.

observed TO phonon mode may be due to misorientation. In fact, according to the relevant symmetry selection rules, the TO phonon mode is forbidden for the (100) face orientation [16]. In practice, however, crystals are often cut ~ 5° off axis for convenience in vapor-phase growth; this slight misorientation is usually enough to allow weak scattering by the forbidden phonons. Another reason for the appearance of the TO mode is that a 90° scattering geometry was used in the measurements [17,18].

Figure 5 illustrates the LO phonon mode changes with the etching time in the mixed acid and the grown oxide film. A strong LO phonon mode, 344 $cm^{-1}$ and a weak TO phonon mode 280 $cm^{-1}$, are observed, both shifted ~ 5 $cm^{-1}$ to lower frequency compared with those measured at mechanically polished surfaces. For the mixed acid etched surface the line shape of the LO phonon mode is narrower than that of the mechanically polished surface indicating the surface damages have been removed by the chemical etching (surface disorder brings about a broadening effect on LO phonon mode). Enhancement of the LO mode intensity was also observed on the p-InP surface etched in the mixed acid for longer etching times. As long as the anodic oxide film was grown at the surface in tartaric acid + propylene glycol, the LO phonon mode intensity decreased and, by contrast, the TO phonon mode intensity increased, as shown in Fig. 5, spectrum c.

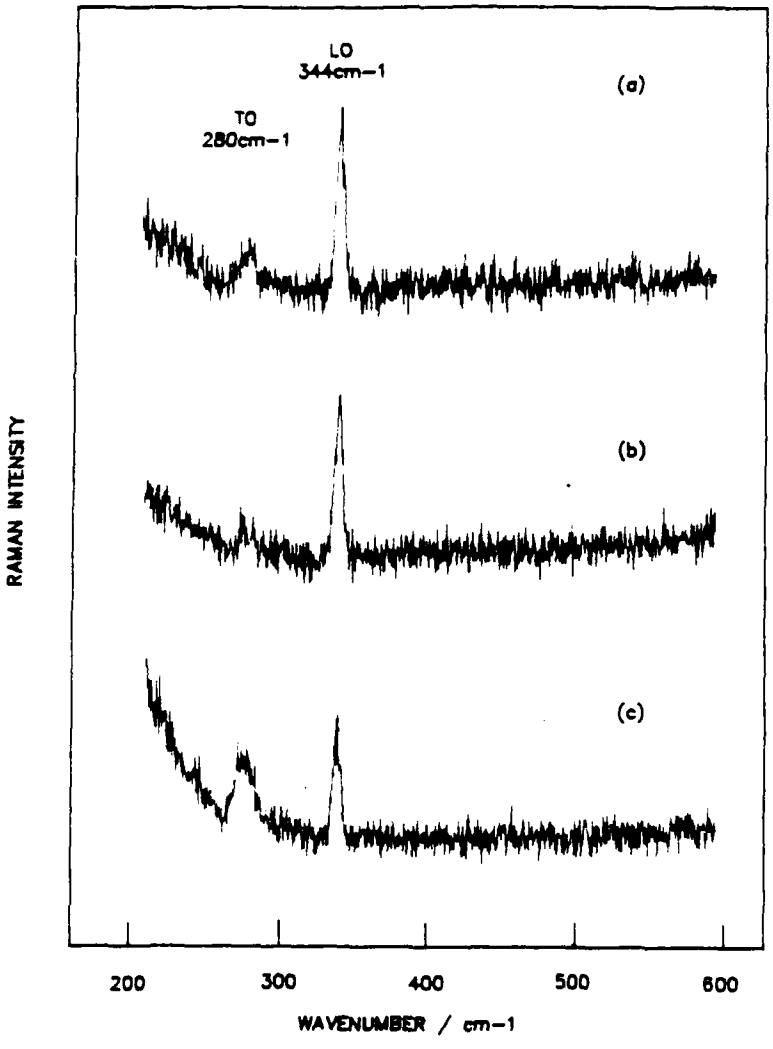


Fig. 5. (a) Same as Fig. 4 except subsequently etched in 6:1:1:1 nitric + perchloric + acetic + hydrochloric acid for 1 min. (b) Same as Fig. 4 except etched for 30 s. (c) Same as Fig. 4 except oxidized in 3% tartaric acid + propylene glycol from −0.4 to +0.7 V vs. SCE after etching in 6:1:1:1 nitric + perchloric + acetic + hydrochloric acid for 30 s.

Raman spectra measured at the $Br_2 + CH_3OH$ etched surface show a decreased intensity of the LO phonon mode compared to that observed at the mixed-acid-etched surface (Fig. 6). The changes in intensity of the LO phonon mode between

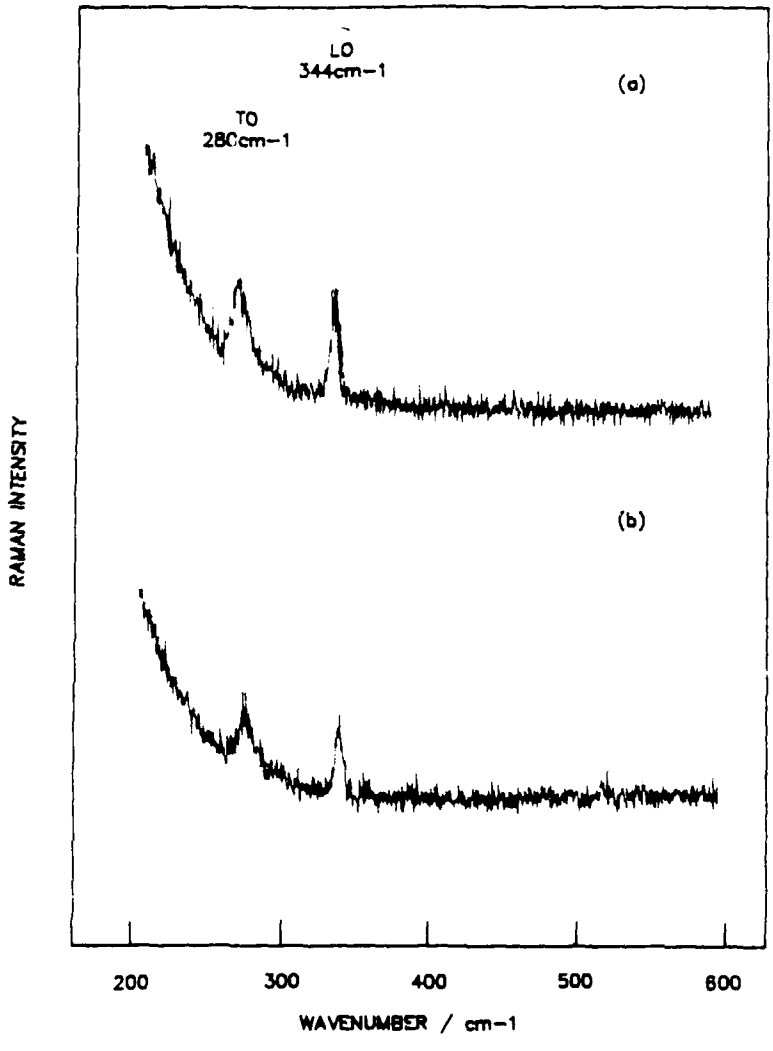


Fig. 6. Same as Fig. 4 except (a) subsequently etched in $Br_2$ + MeOH for 30 s, (b) oxidized in tartaric acid + propylene glycol from −0.4 to +0.7 V after $Br_2 + CH_3OH$ etching.

the surfaces etched in $Br_2 + CH_3OH$ and anodically oxidized in tartaric acid + propylene glycol are not as significant as those observe for the surfaces etched in the mixed acid. In contrast, the intensity of the TO phonon mode is higher (see Figs. 5 and 6).

At the surface of a semiconductor, a space charge region (SCR) may exist in which the density of charge carriers is different from that in the bulk. For optical penetration depths larger than the SCR width, the Raman spectra will show the bands of the coupled modes from bulk as well as the uncoupled LO phonon band from the SCR. Since the p-InP used in experiments has a low doping density, the LO phonon mode observed in Raman scattering spectra is originated from a surface depletion layer at p-InP surfaces provided the Raman scattering from LO phonon in SCR is similar to that in an undoped crystal [18]. The intensity of the unscreened LO phonon, $I(\mathrm{LO})$ can be written as

$$I(\mathrm{LO}) = I_0(\mathrm{LO})\{1 - \exp[-2L_s/d_1(\lambda)]\} \tag{1}$$

where $I_0(\mathrm{LO})$ is the intensity of the LO phonon mode from an undoped semiconductor or a low carrier concentration where the plasmon frequency is too low to affect the LO phonons, $L_s$ is the width of SCR and $d_1(\lambda)$ is the optical skin depth. $L_s$ can be simply expressed as

$$L_s = \left(\frac{2\epsilon_0\epsilon}{eN_d}V_B\right)^{1/2} \tag{2}$$

where $\epsilon_0$ is the permittivity of free space, $\epsilon$ the dielectric constant of semiconductor, $N_d$ the doping density, $e$ the electron charge and $V_B$ the magnitude of the bandbending. It is obvious that the changes in intensity of LO phonon mode reflects the changes in the excess carrier density in SCR and the band bending. Combining eqns. (1) and (2), we can determine the band bending from the Raman scattering spectra if the doping density is known. The Raman scattering spectra were analyzed with eqns. (1) and (2) and the results are given in Table 1. We have taken $N_d$ as $6.0 \times 10^{16}\ \mathrm{cm}^{-3}$ and $d_1$ as 90 nm for InP [19].

Due to the nature of the Raman experiment, it is clear that the technique can only provide information of semiconductor surfaces that are under illumination. There are several consequences; as an example, the bands in SCR may be flattened as a result of the laser illumination, and the band bending may be varied by laser intensity. Therefore, special care was taken in this work with respect to the optical

VARIOUS / Title OK? (If not, please provide more appropriate title)

TABLE 1

Width of space charge region and magnitude of bandbending for ~~differently treated~~ samples

| Samples | | Raman scattering spectroscopy [a] | |
|---|---|---|---|
| | | $L_s$/nm | $V_B$/V |
| Mixed acid etching | etched 30 s | 103.6 | 0.75 |
| | anodic oxidation $-0.3 \rightarrow +0.7$ V vs. SCE | 79.0 | 0.42 |
| $Br_2 + CH_3OH$ etching | etched 30 s | 100.4 | 0.70 |
| | anodic oxidation $-0.3 \rightarrow +0.7$ V vs. SCE | 89.0 | 0.6 |

[a] The intensity of the LO mode at p-InP surface etched in the mixed acid for 1 min was taken as $I_0(\mathrm{LO})$.

alignment and laser power in order to assure that the spectra obtained on subsequent samples were made under the same conditions.

The different surface preparation techniques lead to appreciable differences in band bending in the various samples. The highest intensity of the LO phonon mode was measured at the p-InP surface that had been etched in the mixed acid system for 1 min, indicating that a larger band bending exists in SCR. Etching the p-InP surface in the mixed acid system for a shorter time, say 30 s, produces a weaker LO phonon mode corresponding to a smaller band bending. The dramatic decrease in the intensity of the LO phonon mode at the anodically oxidized surface is attributed to the presence of more free hole density in the SCR and a subsequent decrease in band bending. A smaller reduction in band bending was observed at the anodically oxidized p-InP surface prior to $Br_2 + CH_3OH$ etching.

As mentioned above, the values of band bending obtained from the Raman measurements reflect the values for an illuminated surface, regardless of the band edge position. The observed values for the band bending from these measurements may, however, be compared to those from the capacitance data (which were taken in the dark) since the relative values of change in band bending have been taken into account with respect to different surfaces of InP. It is not surprising that a negative shift of flatband potential at the anodically oxidized p-InP surface responds to a reduction of band bending whether under illumination or in the dark. The Raman scattering data demonstrates the same trends of space charge properties as Mott–Schottky plots.

Many papers have been concerned with the composition of residual oxides formed by either chemical etching [20–23] or of anodically grown oxides [10,24–27] at the surface of p-InP, but the various assignments often conflict. The negative shift of flat-band potential from Mott–Schottky and reduction of the band bending from Raman scattering measurements suggest that the anodix oxide grown in pH 6 tartaric acid + propylene glycol was charged with negative charges. Unfortunately, this anodic oxide at the InP surface was not detected in these experiments by Raman scattering spectroscopy, probably due to the fact that the anodic oxide was not thick enough with respect to the magnitude of the optical skin depth. However, FTIR spectroscopy gave characteristic information regarding the anodic oxide. Figure 7 shows a spectrum which is the ratio of the spectrum taken from an anodically oxidized p-InP surface to that of a surface only etched in the mixed acid. The bands observed in Fig. 7 are listed in the first column of Table 2, and are compared with the literature values of aqueous solution $H_2PO_4^-$ and solid $NaH_2PO_4$ [28]. The bands at 1276 and 1210 $cm^{-1}$ may be assigned to the P–O–H in-plane deformation mode which have been reported at 1280, 1240 and 1098 $cm^{-1}$ in solid $NaH_2PO_4$ and at 1230 $cm^{-1}$ in aqueous $H_2PO_4^-$. The band at 752 $cm^{-1}$ is assigned to the corresponding out-of-plane mode which was observed at 820 $cm^{-1}$ in solid $NaH_2PO_4$. A very weak band at 2912 $cm^{-1}$ and a weak band at 1790 $cm^{-1}$ were observed and may be assigned to water stretching and P–O–H stretching modes. The $PO_2$ symmetrical stretching mode gives a strong band at 1057 $cm^{-1}$ and an antisymmetrical stretch band at 1140 and 1120 $cm^{-1}$. The bands at 987 and 848

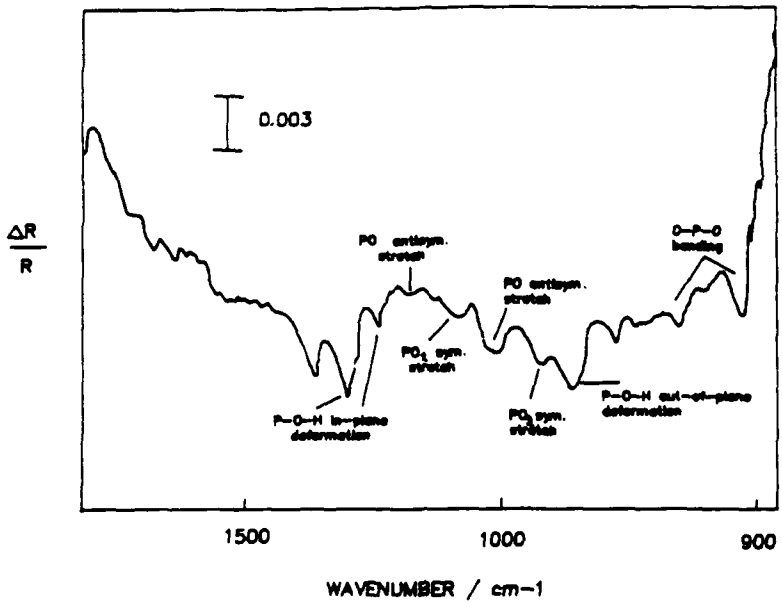


Fig. 7. Surface difference infrared spectrum of the anodically oxidized InP surface referenced to the InP surface etched in the mixed acid system.

TABLE 2

Band ~~assignments for FTIR spectroscopy~~ Assignments

ER

Title OK (if not, please provide a more appropriate title)

| $\nu/cm^{-1}$ | | | ~~Resonance mode~~ Assignment |
|---|---|---|---|
| p-InP surface after anodic oxidation [a] | Aq. soln $H_2PO_4^-$ | Solid $NaH_2PO_4$ | |
| 2912 | 2800–3000 | 2780 | O–H stretching band |
| 1790 | 2880 | 2360 | |
| | 1810 | 1650 | |
| 1276 | | 1280 | |
| 1210 | 1230 | 1240 | P–O–H in plane deformation |
| | | 1098 | |
| 1140 | 1150 | 1166 | $PO_2$ antisymmetrical stretch |
| 1124 | | 1120 | |
| 1057 | 1072 | 1053 | $PO_2$ symmetrical stretch |
| 987 | 947 | 989 | $P(OH)_2$ antisymmetrical stretch |
| | | 932 | |
| 848 | 878 | 875 | $P(OH)_2$ symmetrical PO stretch |
| 752 | | 820 | P–O–H out-of-plane deformation |
| 576 | | 567 | |
| 564 | | 540 | OPO bending mode |
| 507 | | 527 | |
| | | 510 | |

heading OK?

[a] The p-InP was etched in the mixed acid for 60 s prior to anodic oxidation.

$cm^{-1}$ may be regarded as $P(OH)_2$ antisymmetrical and symmetrical PO stretch. It is obvious that those bands observed at the anodically oxidized p-InP surface indicate that the oxidation products formed on the p-InP surface during anodic oxidation are composed of $H_2PO_4^-$ or $IN(H_2PO_4)_3$.

Since there is strong evidence that the surface composition of the oxide depends on the pH of etchants or electrolytes [11,29], it is useful to consider the range of thermodynamic stability of p-InP as a function of pH and of electrode potential. Calculations of the equilibrium potential–pH diagram of p-InP is not available in the literature. Our discussions rely on the individual indium and phosphorus Pourbaix diagrams [30]. Although the hydrated oxide Pourbaix diagrams [30]. Although the hydrated oxide, $In_2O_3 \cdot H_2O$ (or $IN(OH)_3$) is less stable than the anhydrous oxide $In_2O_3$ at pH 5–11, $In_2O_3$ has a minimum solubility at pH 6.9. Its dissolved form below pH 6.9 is $In(OH)^{2+}$ cation which has a tendency to form a solid indium salt with most anions. Phosphorus has a primary oxidation form in pH 2–7.2 as $H_2PO_4^-$. During p-InP anodic oxidation in pH 6 tartaric acid + propylene glycol, the crystal surface could, most likely, be oxidized to $In(H_2PO_4)_3$. This prediction of the appropriate Pourbaix diagrams does indeed agree with our FTIR spectroscopic data. A tentative p-InP oxidation process can thus be suggested as

$$3\ In + 3\ H_2O \rightarrow 3\ (InOH)^{2+} + 3\ H^+ + 9\ e^-$$

$$3\ P + 12\ H_2O \rightarrow 3\ (H_2PO_4)^- + 18\ H^+ + 15\ e^-$$

$$3\ InP + 15\ H_2O \rightarrow IN(H_2PO_4)_5 + 2\ (InOH)^{2+} + 20\ H^+ + H_2O + 24\ e^-$$

$(H_2PO_4)_3$ can, alternately, be written in terms of the oxides:

$$2\ In(H_2PO_4)_3 \rightarrow In_2O_3 + 3\ P_2O_5 + 6\ H_2O.$$

Laughlin and Wilson [10] have reported the ESCA profile of a thick oxide at the p-InP grown in a pH > 3 electrolyte. Their data suggests the outer layer is $In_2O_3$ rich and that there exists an inner region containing a higher concentrations of $P_2O_5$. Thus the ESCA data indicate that the phosphorus is in the $P^{+5}$ oxidation state. This is in agreement with our FTIR spectroscopic data of a thin phosphate surface species formed directly on p-InP lattice in the anodic oxidation process. It is important to realize that the observation of the incorporation of phosphate surface species at p-InP surface can explain the negative shift of flat-band potential. The lattice dangling bonds at the p-InP surface bond with phosphate must result in a charge separation, since one part of the electric change (negative) is localized in phosphate while the counter-charge (positive) remains at the p-InP crystal surface. The amount of electric damage charge is determined by the amount of phosphate species formed on the surface; consequently one observes a negative flat-band shift and a decrease of LO phonon mode intensity.

It should be mentioned that for the p-InP previously etched in $Br_2 + CH_3OH$, the anodically grown phosphate surface species shows the same infrared spectrum, but the intensity of the characteristic bands were reduced. This is an indication that less

phosphate was probably formed on the surface. This trend is consistent with the Raman scattering results (where the LO phonon mode only exhibited a small reduction intensity compared with that etched in the $Br_2 + CH_3OH$) and the Mott–Schottky plots (where a less negative shift in flat-band potential is shown) which will be discussed in a later section.

Various etchants have been used to remove oxide layers at the p-InP surface. For example, HF etchant gives fairly clean and stable InP surfaces [29] and HCl etches InP under the action of the $Cl^-$ ion with phosphorus, and the subsequent removal of phosphorous from the surface [22]. On the other hand, Br-based etchants leave phosphorus-rich oxide traces [29]. The 2% $Br_2 + CH_3OH$ etchant solution used in this work might not only remove the mechanically damaged surface but also introduce p-rich oxide traces on the surfaces corresponding to a lower intensity of LO phonon mode and a less positive flat-band potential relative to that of the surfaces produced by the mixed etchant solutions. However, this trace oxide has a thickness ranging from 0.4 to 0.7 nm and a characteristically discontinuous surface structure [20]. This is confirmed by the electrical properties of the photocathode, which behaved as an almost ideal Schottky junction in acetonitrile although a small hysteresis on the capacitance curve was observed due to the instability of the oxide trace. For the mixed acid (6 : 1 : 1 $HNO_3 + HCl + HClO_4$ $CH_3COOH$) etchant, we propose that a fairly oxide-free p-InP surface is efficiently produced which leads to large values of bandbending. The anodic phosphate film (or P-rich oxide) on the surface etched with the mixed acids is suggested to be a continuous layer which results in the formation of a semiconductor/oxide/electrolyte structure (like a MOS device) for the InP photocathode.

Comparing the TO phonon mode intensities of the mixed acid, $Br_2 + CH_3OH$ etched and anodically oxidized p-InP surfaces, we found the higher TO mode was resolved from $Br_2 + CH_3OH$ etched and anodically oxidized surfaces. The TO phonons are not accompanied by a long-range electrical field; thus they do not couple directly to the plasma oscillations and are unaffected by change in excess carrier density [31]. The TO phonon mode would, however, be affected by structural bonding, while the LO mode intensity and line width have an additional contribution due to third order non-linear susceptibility [32]. The enhancement of the TO phonon mode on $Br_2 + CH_3OH$ etched and anodically oxidized p-InP surfaces is probably due to the formation of phosphorus-rich oxide, which induced a modification of structural bonding and a difference of thermal expansion between phosphate and InP. The InP surface may, therefore, be partially inclined toward another crystal face (such as (110)) which allows transition of the TO phonon mode.

It was also found that the InP surface was contaminated by carbon after etching either in acids or $Br_2$-based etchants. According to Singh et al. [33] the Auger studies have shown that the $Br_2 + CH_3OH$ etched surface is more contaminated with C and O than acid etched surfaces. There is no evidence at this time that carbon contamination has any affect on the electrical characteristics of the semiconductor system [29].

The anodically oxidized InP surface previously etched in $Br_2 + CH_3OH$ showed

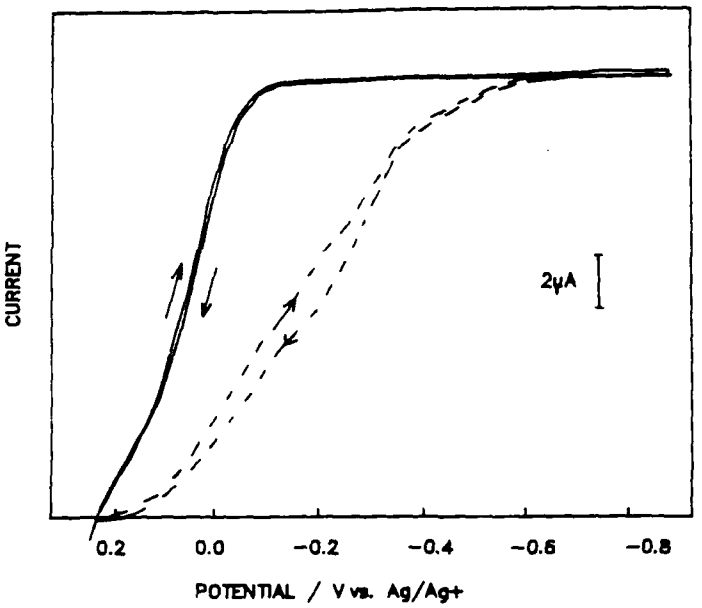


Fig. 8. Photocurrent–voltage curves for p-InP in 0.1 *M* TBAF containing 5 m*M* TCNQ. The solid curve is that of the surface etched in the mixed acid, and the dashed curve is that of the anodically oxidized surface. The curves were measured by the phase sensitive detection method at a frequency of 80 Hz.

evidence of a small reduction in bandbending from the behavior of the LO phonon mode and a smaller shift in flatband potential from the Mott–Schottky plots. This behavior may very well involve the severe C and O contamination which could play an important role in the morphology of the surface layer formed during the surface anodic oxidation. On one hand, carbon may block oxidation sites on the InP surface. In fact, the anodic oxidation current at $Br_2 + CH_3OH$ etched surfaces was one third smaller than that observed on the mixed acid etched surface. On the other hand, phosphate may grow directly on P-rich oxide traces resulting in an island structure during anodic oxidation. Although this phosphate is discontinuous, it is possible that it has good electric properties since it is only the expansion of the P-rich oxide trace formed in $Br_2 + CH_3OH$ etching. (There could be less mismatch of the bonding between the InP lattice and growing phosphate, which can become surface states.) At some stage in the oxidation, phosphate growth would change from one-dimensional growth to two-dimensional growth. At this point, the "islands" would begin to contract leaving flaws.

Figure 8 compares the photocurrent–voltage curves measured from the mixed acid etched and the anodically oxidized InP surfaced by the lock-in phase sensitive detection method at $\lambda = 700$ nm in 0.1 *M* TBAF + acetonitrile solution with 5 m*M* tetracyanoquinodimethane as a redox couple. For the mixed acid etched surface, the

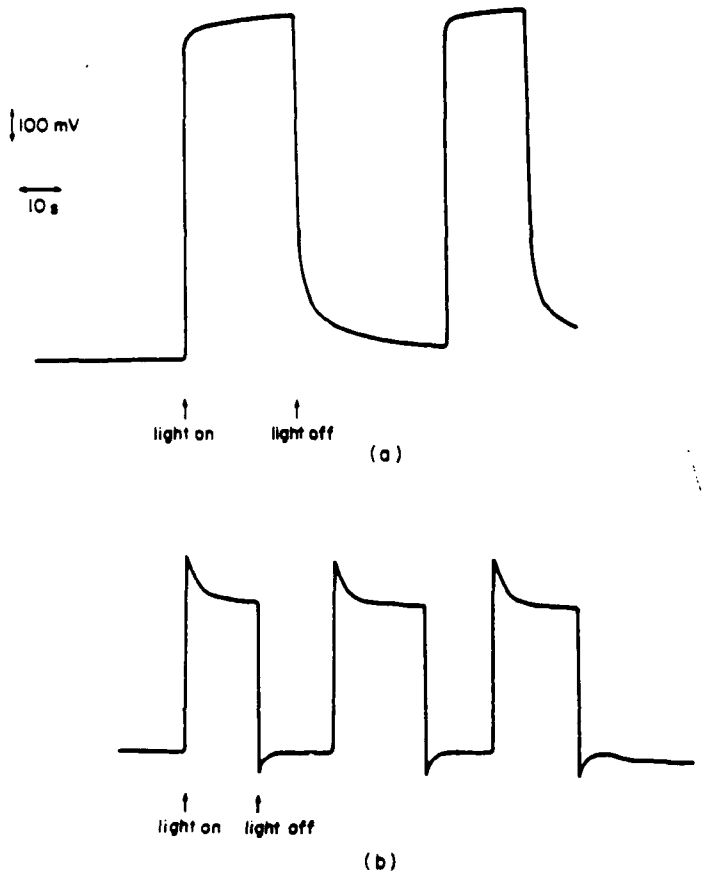


Fig. 9. Open circuit photovoltage measured in 5 m*M* TCNQ + 0.1 *M* TBAF + acetonitrile at p-InP (a) etched in 6:1:1:1 nitric + perchloric + acetic + hydrochloric acid for 1 min and (b) oxidized in tartaric acid + propylene glycol.

photocurrent rose steeply to saturation after its potential was swept across the flat-band potential. In contrast, the onset of the photocurrent at the anodically oxidized InP was delayed and the photocurrent increased with the potential slowly. In addition, the hysteresis on the curve between the forward and reverse scans was unambiguous. Figure 9 presents the open circuit photovoltage measured from the mixed acid etched and the anodically oxidized InP surfaces. A significant open-circuit photovoltage reduction, − 350 mV, was also observed, which coincides with the values of reduction of the bandbending evident from the Raman scattering spectra. The photocurrent onset potential delay and slow photocurrent increase with potential are some of the characteristic features of the recombination of minority carriers

via surface states [34]. The surface states were introduced on the InP surface along with the phosphate formation. They may arise because of the mismatch between InP and phosphate species that leaves dangling bonds or other non-bonding orbitals at the semiconductor surface. The photoelectrochemical properties of InP/oxide/electrolyte systems can be dominated by such surface states if they are present at sufficient surface density. For example, surface states may pin the Fermi level. The origin of the plateau on Mott–Schottky plots and changes in the behavior of photocurrent and photovoltage is attributed to the surface state brought about P-rich oxide present on the InP surface. We estimate the surface state density on InP/oxide from the data of shift in flat-band potential, to be on the order $3 \times 10^{13}$ $cm^{-2}$. More details of the results of studies on surface recombination of InP/oxide will be reported in a subsequent report.

ACKNOWLEDGEMENT

The authors thank the Office of Naval Research for support of part of this work.

REFERENCES

1 A. Heller, R.G. Vadimsky, W.P. Johnson, Jr., K.E. Strege, H.J. Leamy and B. Miller, Conf. Rec. IEEE Photovoltaic Spec. Conf., 15 (1981) 1422; A. Heller, E. Aharon-Shalom, W.A. Bonner and B. Miller, J. Am. Chem. Soc. 104 (1982) 2942.
2 A. Heller, B. Miller and F.A. Thiel, Appl. Phys. Lett., 38 (1981) 282.
3 D.L. Lile and D.A. Collins, Appl. Phys. Lett., 28 (1976) 554.
4 J.P. Wager and C.W. Wilmsen, J. Appl. Phys., 51 (1980) 812.
5 D.L. Lile, D.A. Collins, L.G. Meiners and L. Messick, Electron. Lett., 14 (1978) 657.
6 T. Kawakami and M. Okamura, Electron. Lett., 15 (1979) 502.
7 R.F.C. Farrow, J. Phys. D., 7 (1974) 2435.
8 H.J. Lewerenz, D.E. Aspnes, B. Miller, D.L. Malm and A. Heller, J. Am. Chem. Soc. 104 (1982) 3325.
9 See for example: C.W. Wilmsen and R.W. Kee, J. Vac. Sci. Technol., 14 (1977) 953; 15 (1978) 1513; K.M. Geib and C.W. Wilmsen, J. Vac. Sci. Technol., 17 (1980) 952.
10 D.H. Laughlin and C.W. Wilmsen, Appl. Phys. Lett., 37 (1980) 915.
11 A. Yamamoto, M. Yamaguchi and C. Uemura, J. Electrochem. Soc., 129 (1982) 2795.
12 M. Sakashita, T. Ohtsuka and N. Sato, J. Electrochem. Soc., 132 (1985) 1864.
13 See for example: H. Shen and F.H. Pollak, Appl. Phys. Lett., 45(6) (1984) 692; 47(8) (1985) 891; D.R. Myers and P.L. Gourley, J. Electrochem. Soc., 130 (1983) 217.
14 T. Nakamura and T. Katoda, J. Appl. Phys., 55 (1984) 3064.
15 See for example: A Bewick and S. Pons, in C. Hester (Ed.), Advances in Infrared and Raman Spectroscopy, Hayden and Sons, London, 1985, p. 1; J. Foley and S. Pons, Anal. Chem., 57 (1985) 945A.
16 M. Cardona in M. Cardona and G. GUntherodt (Eds.) Light Scattering in Solids, Vol. 2, Springer, New York, 1982.
17 K. Murase, S. Katayama, H. Kawamura and Y. Ando, Prog. Theor. Phys., 57 (1975) 115.
18 A. Pinczuk, A.A. Ball, R.E. Nahory, M.A. Pollack and J.M. Woolock, J. Vac. Sci. Technol., 16 (1979) 1168.
19 D.E. Aspnes and A.A. Studna, Phys. Rev., 27 (1983) 985.
20 D.T. Clark, T. Fok, G.G. Roberts and R.W. Sykes, Thin Solid Films, 70 (1980) 261.
21 P.W. Chye, I. Lindan, P. Pianetta, C.M. Garner, C.Y. Su and W.E. Spicer, Phys. Rev., 818 (1978) 5545.

22 P.A. Bertrand, J. Vac. Sci. Technol., 18 (1981) 28.
23 J.F. Wager, D.L. Ellsworth, S.M. Goodnick and C.W. Wilmsen, J. Vac. Sci. Technol., 19 (1981) 513.
24 K.M. Geibs and C.W. Wilmsen, J. Vac. Sci. Technol., 17 (1980) 952.
25 J.E. Griffiths, G.P. Schwartz, W.A. Sunder and H. Schonhorm, J. Appl. Phys., 53 (1982) 1832.
26 M. Yamaguchi, J. Appl. Phys., 53 (1982) 1834.
27 L.L. Kazmerski, P.J. Freland, P. Sheldon, T.L. Chu, S.S. Chu and C.L. Lin, J. Vac. Sci. Technol., 17 (1980) 1061.
28 A.C. Chapman and L.E. Thirlwell, Spectrochim. Acta, 20 (1964) 937.
29 A. Guivarch, H.L. Haridon and G. Pelous, J. Appl. Phys., 55 (1984) 1139.
30 M. Pourbaix, Atlas of Electrochemical Equilibria in Aqueous Solutions, Pergamon Press, Oxford, 1966.
31 A. Mouradian and A.L. McWhorter in G.B. Wright (Ed.), Light Scattering Spectra of Solids, Springer New York, 1968, p. 297.
32 T. Karmijoh, H. Takano and M. Sakuta, J. Appl. Phys., 55 (1984) 3756.
33 S. Singh, R.S. Williams, L.G. Van Uiters, A. Schlierr, I. Camlibel and W.A. Bonner, J. Electrochem. Soc., 130 (1982) 447.
34 See for example: L.M. Peter, J. Li and R. Peat, J. Electroanal. Chem., 165 (1984) 29; R.H. Wilson, J. Appl. Phys., 48 (1977) 4292; F. El Guibaly and K. Colbow, J. Appl. Phys., 53 (1982) 1737.

DL/1113/87/2

# TECHNICAL REPORT DISTRIBUTION LIST, GEN

| | No. Copies |
|---|---|
| Office of Naval Research<br>Attn: Code 1113<br>800 N. Quincy Street<br>Arlington, Virginia 22217-5000 | 2 |
| Dr. Bernard Douda<br>Naval Weapons Support Center<br>Code 50C<br>Crane, Indiana 47522-5050 | 1 |
| Naval Civil Engineering Laboratory<br>Attn: Dr. R. W. Drisko, Code L52<br>Port Hueneme, California 93401 | 1 |
| Defense Technical Information Center<br>Building 5, Cameron Station<br>Alexandria, Virginia 22314 | 12 high quality |
| DTNSRDC<br>Attn: Dr. H. Singerman<br>Applied Chemistry Division<br>Annapolis, Maryland 21401 | 1 |
| Dr. William Tolles<br>Superintendent<br>Chemistry Division, Code 6100<br>Naval Research Laboratory<br>Washington, D.C. 20375-5000 | 1 |
| Dr. David Young<br>Code 334<br>NORDA<br>NSTL, Mississippi 39529 | 1 |
| Naval Weapons Center<br>Attn: Dr. Ron Atkins<br>Chemistry Division<br>China Lake, California 93555 | 1 |
| Scientific Advisor<br>Commandant of the Marine Corps<br>Code RD-1<br>Washington, D.C. 20380 | 1 |
| U.S. Army Research Office<br>Attn: CRD-AA-IP<br>P.O. Box 12211<br>Research Triangle Park, NC 27709 | 1 |
| Mr. John Boyle<br>Materials Branch<br>Naval Ship Engineering Center<br>Philadelphia, Pennsylvania 19112 | 1 |
| Naval Ocean Systems Center<br>Attn: Dr. S. Yamamoto<br>Marine Sciences Division<br>San Diego, California 91232 | 1 |

DL/1113/87/2

ABSTRACTS DISTRIBUTION LIST, SDIO/IST

Dr. Robert A. Osteryoung
Department of Chemistry
State University of New York
Buffalo, NY 14214

Dr. Douglas N. Bennion
Department of Chemical Engineering
Brigham Young University
Provo, UT 84602

Dr. Stanley Pons
Department of Chemistry
University of Utah
Salt Lake City, UT 84112

Dr. H. V. Venkatasetty
Honeywell, Inc.
10701 Lyndale Avenue South
Bloomington, MN 55420

Dr. J. Foos
EIC Labs Inc.
111 Downey St.
Norwood, MA 02062

Dr. Neill Weber
Ceramatec, Inc.
163 West 1700 South
Salt Lake City, UT 84115

Dr. Subhash C. Narang
SRI International
333 Ravenswood Ave.
Menlo Park, CA 94025

Dr. J. Paul Pemsler
Castle Technology Corporation
52 Dragon Ct.
Woburn, MA 01801

Dr. R. David Rauh
EIC Laboratory Inc.
111 Downey Street
Norwood, MA 02062

Dr. Joseph S. Foos
EIC Laboratories, Inc.
111 Downey Street
Norwood, Massachusetts 02062

Dr. Donald M. Schleich
Department of Chemistry
Polytechnic Institute of New York
333 Jay Street
Brooklyn, New York 01

Dr. Stan Szpak
Code 633
Naval Ocean Systems Center
San Diego, CA 92152-5000

Dr. George Blomgren
Battery Products Division
Union Carbide Corporation
25225 Detroit Rd.
Westlake, OH 44145

Dr. Ernest Yeager
Case Center for Electrochemical Science
Case Western Reserve University
Cleveland, OH 44106

Dr. Mel Miles
Code 3852
Naval Weapons Center
China Lake, CA 93555

Dr. Ashok V. Joshi
Ceramatec, Inc.
2425 South 900 West
Salt Lake City, Utah 84119

Dr. W. Anderson
Department of Electrical & Computer Engineering
SUNY - Buffalo
Amherst, Massachusetts 14260

Dr. M. L. Gopikanth
Chemtech Systems, Inc.
P.O. Box 1067
Burlington, MA 01803

Dr. H. F. Gibbard
Power Conversion, Inc.
495 Boulevard
Elmwood Park, New Jersey 07407

DL/1113/87/2

ABSTRACTS DISTRIBUTION LIST, SDIO/IST

Dr. V. R. Koch
Covalent Associates
52 Dragon Court
Woburn, MA 01801

Dr. Randall B. Olsen
Chronos Research Laboratories, Inc.
4186 Sorrento Valley Blvd.
Suite H
San Diego, CA 92121

Dr. Alan Hooper
Applied Electrochemistry Centre
Harwell Laboratory
Oxfordshire, OX11 ORA UK

Dr. John S. Wilkes
Department of the Air Force
The Frank J. Seiler Research Lab.
United States Air Force Academy
Colorado Springs, CO 80840-6528

Dr. Gary Bullard
Pinnacle Research Institute, Inc.
10432 N. Tantan Avenue
Cupertino, CA 95014

Dr. J. O'M. Bockris
Ementech, Inc.
Route 5, Box 946
College Station, TX 77840

Dr. Michael Binder
Electrochemical Research Branch
Power Sources Division
U.S. Army Laboratory Command
Fort Monmouth, New Jersey 07703-5000

Professor Martin Fleischmann
Department of Chemistry
University of Southampton
Southampton, Hants, SO9 5NH UK